ACS Energy LETTERS

http://pubs.acs.org/journal/aelccp

A Polysiloxane-Enabled Ternary Eutectic Electrolyte with Fast Ion Transport under Extreme Conditions

Weiping Li, Peng Wen, Yang Ren, Wen Xie, Jun Lin, Mao Chen, Yuan Yang,* and Xinrong Lin*

Cite This: *ACS Energy Lett.* 2023, 8, 5128−5135

Read Online

ACCESS | Metrics & More | Article Recommendations | Supporting Information

ABSTRACT: **Developing lithium−metal batteries under extreme conditions is highly challenging and requires flammable/volatile solvents. In pursuit of safe electrolyte materials, polymers possess slow lithium transport, while eutectic electrolytes (EEs) suffer from interfacial instability, impeding their applications under extreme conditions. Herein, we report that addition of a designed brush-polysiloxane into EE unexpectedly boosted ionic conductivity by nearly 3-fold to 0.59 mS cm^{-1} at −40 °C compared to that without polymer, fulfilling fast transport kinetics. Spectroscopic characterizations and simulations revealed formation of a ternary EE via intermolecular interactions as well as a stabilized interface, which successfully led to a high capacity of 149 mAh g^{-1} at −40 °C (85% of room-temperature capacity) and stable fast-charging performance up to 1,000 mA g^{-1} (6 min recharging) over 100 cycles in Li||LiNi$_{0.6}$Co$_{0.2}$Mn$_{0.2}$O$_2$ cells. The polymer-enhanced electrolyte offers a paradigm shift approach to tune kinetics in high-performance and safe lithium batteries under extreme conditions.**

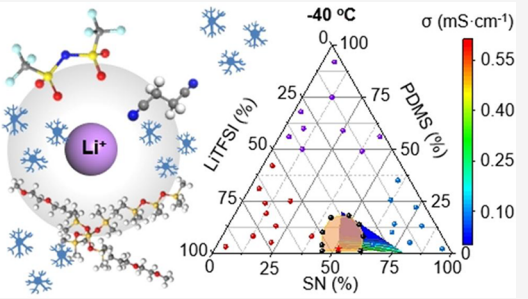

The development of rechargeable lithium batteries under extreme conditions is critical to enable high-performance energy storage for cutting-edge applications such as electric vehicles, aerospace, and underwater exploration.[1−3] In particular, replacing conventional graphite with Li anode to access lithium metal batteries (LMBs) is of interest to achieve energy density beyond 300 Wh kg^{-1}.[4] Unfortunately, LMBs are known to suffer from substantial energy loss at low temperatures (low-T) or high-rate. For instance, only 5−10% of room-temperature capacity is retained at −40 °C;[5] high power capability above 2 C-rates is rather limited.[6] These challenges to a large degree originate from difficult Li$^+$ transport in bulk electrolyte,[7] as well as high charge transfer barrier of Li$^+$ at the electrolyte/electrode interface.[8,9] Furthermore, exacerbated lithium dendrites and interfacial instability at such conditions impose safety concerns.[5]

To accelerate Li$^+$ solvation kinetics, significant efforts have been devoted to small molecules that are low-freezing or low-solvating. For example, liquefied gas was exploited as electrolyte under pressure at −60 °C.[10] A variety of ethers,[8] carbonates,[11] esters,[12] fluorinated solvents,[13] and liquid hydrocarbons[14] were used at ultralow temperatures, providing reserved capacity 50−80% of that at room-temperature. Despite these important advances, flammability and volatility remain issues in state-of-the-art electrolytes. In pursuit of ion-conductive and nonflammable electrolytes for LMBs, eutectic electrolytes (EE) have emerged as novel electrolyte materials by forming eutectics between a solid crystal such as succinonitrile (SN) with lithium salts, offering safety while providing fast ion transport.[15−18] Nevertheless, EE could contain reactive groups that are chemically incompatible with Li, prohibiting reversible battery cycling.[19] Beyond eutectic electrolytes, polymers are attractive electrolyte compositions owing to their thermal and chemical stability.[20−27] However, at low-T or high-rates, polymers are poor ion conductors because their conductivities are several orders of magnitude lower than that of solvents.[2] Even though polymers have been found to be able to alleviate degradation of polar solvents[28] and weaken solvation of Li$^+$,[29] most of them are highly viscous or (semi)crystalline. Thus, the doping/use of polymers typically retards ionic transport, particularly impeding dynamically challenging conditions.

Herein, we report a polymer-enabled ternary eutectic electrolyte (ternary EE) that showed unexpected ion transport behavior at low-T and high-rate conditions. Distinct from

Received: July 31, 2023
Revised: November 1, 2023
Accepted: November 13, 2023

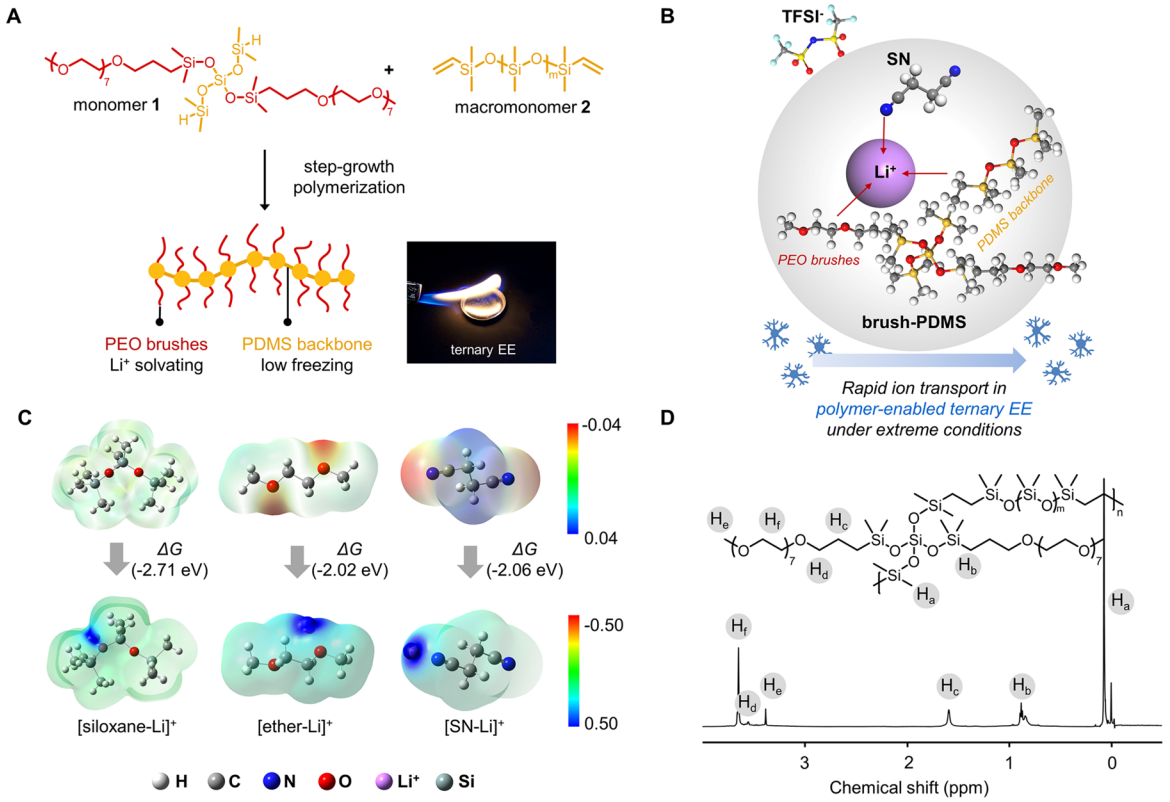

Figure 1. (A) Synthesis of brush-PDMS and nonflammability of ternary EE. (B) Schematic of formation of a polymer-enabled ternary EE. (C) Molecular electrostatic potential mapping and free energy change after formation between characteristic electrolyte segments and Li^+. (D) ^1H spectrum of brush-PDMS.

previous studies that exploit ternary EE among small molecules,[30] we enabled the formation of a ternary EE between bis(trifluoromethanesulphonyl)imide (LiTFSI), SN, and a unique brush-polydimethylsiloxane polymer (brush-PDMS), based on intermolecular Lewis acid−based interactions as revealed via spectroscopic and theoretical analysis. More importantly, doping only 2 wt% of brush-PDMS polymer, instead of slowing down ion transport, enabled nearly tripled ionic conductivity compared to that without polymer. Hence, we achieved high conductivity of 0.59 mS cm^{-1} at −40 °C and stable Li deposition over 3,000 h at areal capacity of 30.0 mAh cm^{-2} or −10 °C. In addition, the ternary EE afforded high capacities of 149 mAh g^{-1} at −40 °C (85% of room-temperature capacity) in assembled Li||Li-$Ni_{0.6}Co_{0.2}Mn_{0.2}O_2$ (NCM622) cells and fast-charging performance up to 1,000 mA g^{-1} (6 min recharging time) over 100 cycles with high initial capacity of 96 mAh g^{-1}. The intriguing finding of polymer-enabled ternary eutectic electrolyte could shed light on novel and safe electrolyte discovery leveraging polymers and foster deeper understanding of tuning kinetics in lithium batteries.

Synthesis of Brush-PDMS and Improved Ion Transport in Ternary EE. PDMS among polymers, are of potential to be low-freezing electrolytes owing to the excellent flexibility of the −SiO− backbone.[31] However, their battery cycling has gained rare success because they are poor at solvating lithium salts and tend to phase separate with other solvents. Therefore, we designed a brush-PDMS structure bearing a PDMS backbone grafted with PEO pendants as shown in Figure 1A. While the interactions between SN and LiTFSI in an eutectic electrolyte are well-established,[32] we envisioned that the binding between PDMS and Li^+ could enable the formation of a PDMS-SN-LiTFSI ternary EE (Figure 1B), which would synergistically facilitate Li^+ mass transport, minimize phase separation, and shield parasitic reactions between SN and Li anode, thereby yielding polymer composite electrolytes functioning at dynamically challenging conditions. To test this hypothesis, we first performed density functional theory (DFT) analysis to simulate electrostatic potentials and calculate formation energies in terms of free energy change (ΔG) between the characteristic electrolyte segments and Li^+ ions (Figure 1C, eqs S1 and S2). It was found that siloxane segments in PDMS exhibit favorable donor behavior of a Lewis base that is comparable to PEO despite of their low dielectric constant,[32] presumably benefitting from connectivity with electron-donating methyl groups. This has led to an $\Delta G_{[\text{siloxane-Li}^+]}$ slightly higher (−2.71 eV) than those of ether segments in PEO (−2.02 eV) and SN (−2.06 eV). Such intermolecular coordination between polymer segments and lithium salts has been previously observed in fluoropolymer electrolytes.[33]

Two polyether chains as alternating brushes on PDMS backbone were then experimentally incorporated to improve phase compatibility while allowing lateral polymer chain propagation (Schemes S1−S5, Figures S1−S5).[34] The brush-PDMS polymer was synthesized via step-growth copolymerization with PEO-functionalized Si−H terminated siloxane (monomer **1**) and divinyl-substituted PDMS (macromonomer **2**). As shown in Figure 1D, the presence of proton signals from H_a to H_f and the absence of vinyl protons in nuclear magnetic resonance (NMR) confirmed the generation of brush-PDMS and the full conversion of **2**. The disappearance of the Si−H

https://doi.org/10.1021/acsenergylett.3c01558
ACS Energy Lett. 2023, 8, 5128−5135

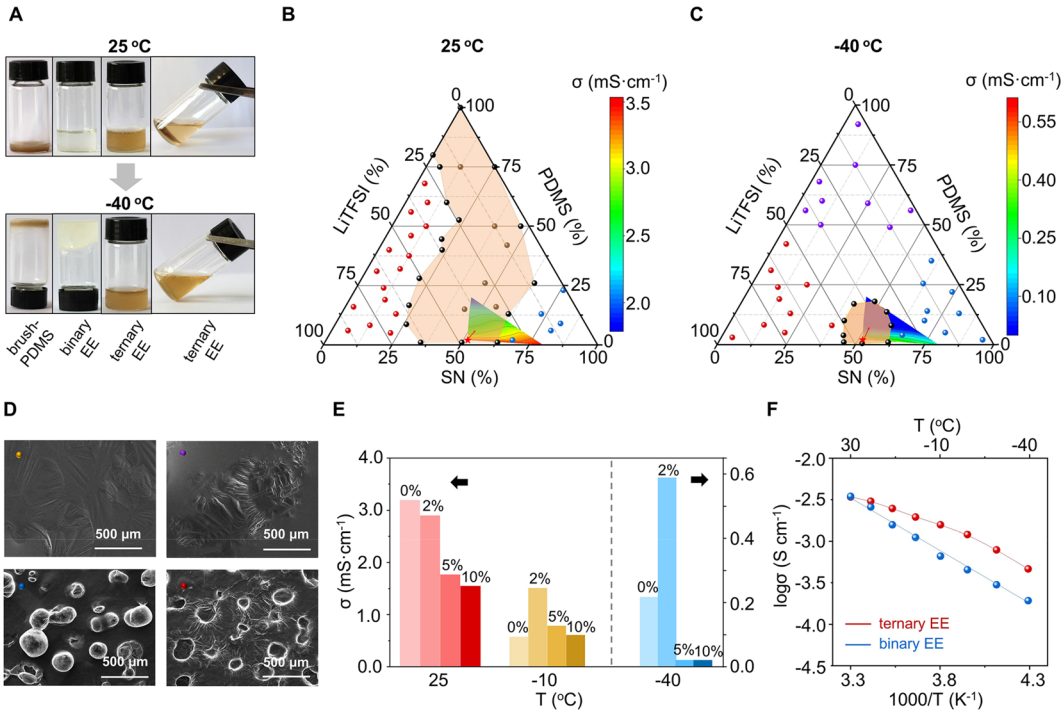

Figure 2. (A) Optical image of PDMS-SN-LiTFSI ternary EE at 25 °C and −40 °C. Ternary phase diagram of PDMS-SN-LiTFSI at (B) 25 and (C) −40 °C. Orange area: isotropic liquid; red points: LiTFSI salt; blue points: SN crystal; purple points: polymer crystal. (D) SEM characterization of different phases in PDMS-SN-LiTFSI. (E) Ionic conductivities of ternary EE with different concentrations of brush-PDMS polymer at varied temperatures. (F) Temperature-dependent ionic conductivity of ternary EE.

stretching vibration at 2140 cm^{-1} in Fourier transform infrared (FT-IR) spectroscopy validated the complete consumption of monomer **1** (Figure S6).

The as-synthesized brush-PDMS was a liquid at ambient temperature with limited ionic conductivity (Figures S8 and S9). SN-LiTFSI binary eutectic electrolyte (binary EE) was used as a baseline electrolyte, with fluoroethylene carbonate (FEC) as an additive to promote formation of stable SEI.[13] Brush-PDMS was added to binary EE to prepare ternary EE, with other compositions kept identical to investigate the role of polymer. While the ternary EE composed of succinonitrile (SN), lithium bis(trifluoromethanesulfonyl) imide (LiTFSI), and brush-PDMS was a transparent liquid at 25 °C, it remained in a liquid state as low as −40 °C, despite the respective freezing of brush-PDMS and binary EE at low temperatures, indicating the formation of ternary eutectics (Figure 2A). Different percentages of brush-PDMS, SN, and LiTFSI were varied using a triangle phase diagram as the design scheme to locate the isotropic eutectic liquid phase at different temperatures (Figure 2B,C). The shadowed area in orange indicates the isotropic liquid regime, while crystalline morphologies suggest noneutectic compositions via scanning electron microscopy (SEM, Figure 2D). At 25 °C, SN and LiTFSI formed eutectics at ratios from 36:64 to 63:37 wt% (SN: LiTFSI), consistent with a literature report.[28] Adding brush-PDMS to binary EE formed ternary eutectics in a wide range of brush-PDMS amounts from 1.0 to 100 wt%, which reduced conductivity from 3.2 mS cm^{-1} (binary EE without brush-PDMS) to 2.9 mS cm^{-1} (binary EE with 2 wt% of brush-PDMS) and 1.6 mS cm^{-1} (binary EE with 10 wt% of brush-PDMS), showing a normal behavior by doping viscous polymer into a solvent (Figure 2E).[2,21]

Surprisingly, at −40 °C, blending brush-PDMS with the SN-LiTFSI binary EE resulted in a transformation from a solid to uniform liquid. Even though only present in a narrow region, a ternary eutectic mixture was formed when the amount of brush-PDMS was varied from 0.5 to 18 wt%. Also, the formation of liquid eutectic afforded a reversed trend of conductivity. For example, doping brush-PDMS of 2 wt% more than doubled the ionic conductivity of binary EE at −10 °C (1.5 vs 0.57 mS cm^{-1}). At −40 °C, an even more evident 3-fold increase (0.59 vs 0.21 mS cm^{-1}) was observed, benefitting from formation of a ternary eutectic electrolyte. We further identified that the ternary eutectics regime was situated at 0.5−18 wt% of brush-PDMS addition, with the conductivity peaked at 2 wt%. Continued increment of brush-PDMS to 10 wt% at −40 °C decreased conductivity to 0.02 mS cm^{-1}, whereby ternary eutectics remained but were subjected to typical conductivity reduction scaling with the amount of viscous polymer. Of note, as opposed to binary EE that showed a linear temperature dependence of conductivity, the favorable ion transport of ternary EE at low-T was better fitted by the Vogel−Tammann−Fulcher (VTF, eq S8 and Table S1) equation with nonlinear relationship due to ion hopping involving motion of polymeric chains (Figure 2F).[35] Diffusion coefficient simulated by molecular dynamics (MD, Figure S10) as well as measured via pulsed gradient spin echo nuclear magnetic resonance (PGSE-NMR; Figures S11 and S12, Table S2) further supported the reversed trend of ion transport at low temperatures. Taken together, 2 wt% of brush-PDMS was chosen to formulate ternary EE, which afforded high conductivity of 2.9 mS cm^{-1} at 25 °C and 0.59 mS cm^{-1} at −40 °C with nonflammability (Figure 1A), electrochemical stability (Figure S13), phase compatibility, and Li interfacial

https://doi.org/10.1021/acsenergylett.3c01558
ACS Energy Lett. 2023, 8, 5128−5135

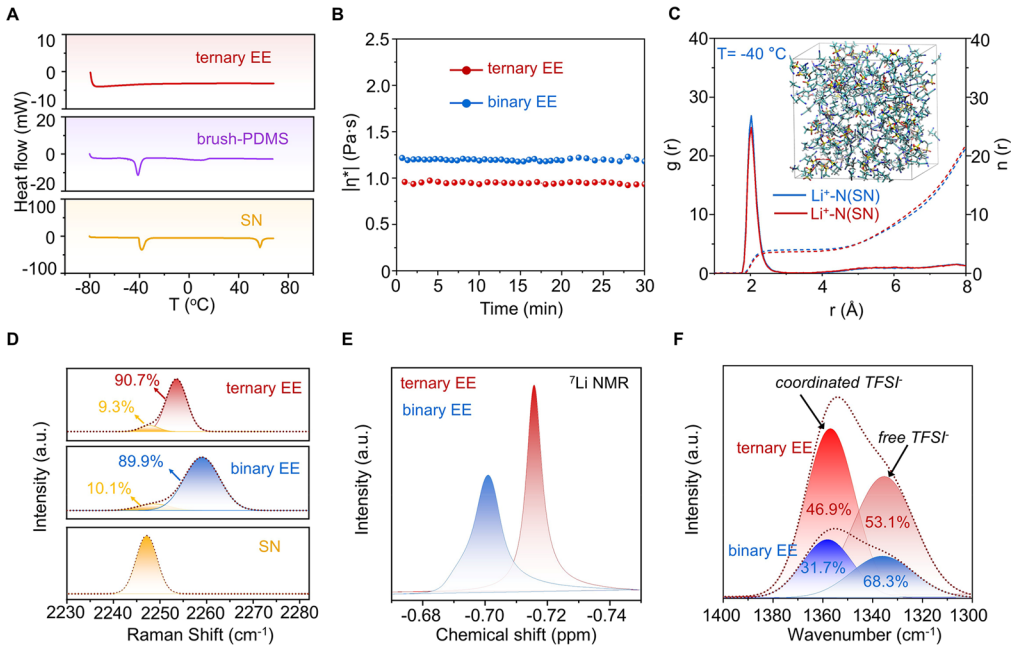

Figure 3. (A) Ternary eutectic behavior characterized by DSC. (B) Viscosity comparison between ternary EE and binary EE via rheological measurement at 25 °C (strain γ = 1%, frequency = 1 Hz). (C) Molecular dynamics simulation of RDF ($g(r)$, solid lines) and coordination numbers ($n(r)$, dashed lines) for Li^+-N (red: ternary EE; blue: binary EE) at −40 °C. Coordination environment change characterized by (D) Raman spectra, (E) ^{7}Li NMR, and (F) FT-IR.

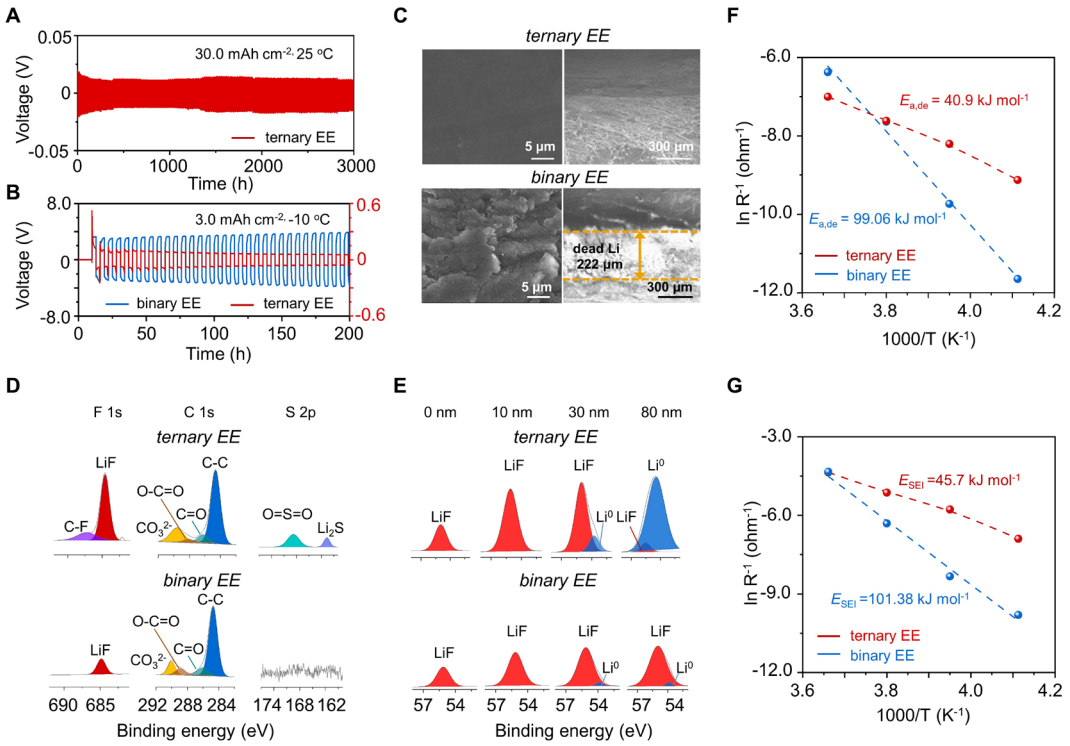

Figure 4. Li stripping/plating tests in Li||Li cells with (A) 30.0 mAh cm^{-2} at 25 °C and (B) −10 °C at 3.0 mAh cm^{-2}. (C) Morphology of the Li deposition layer by top-view and cross-sectional view after cycling at −10 °C for 200 h. (D) SEI composition (sputtering depth = 30 nm) and (E) thickness of SEI probed by XPS after cycling at −10 °C for 200 h. Activation energy of (F) Li^+ desolvation and (G) Li^+ migration across SEI was characterized by EIS.

stability (Figures S14−S16), as well as high lithium transference number (Figure S17).

Formation Mechanism and Solvation in Ternary EE. The formation of a ternary eutectic electrolyte was attributed to the intermolecular interactions among the three compositions based on Lewis acid−base interactions between Li^+ ions and electron-donating −SiO− and C≡N groups, which could overcome molecular packing and prevent formation of crystallization domains. To probe the intermolecular interactions between brush-PDMS, LiTFSI, and SN, differential

https://doi.org/10.1021/acsenergylett.3c01558
ACS Energy Lett. 2023, 8, 5128−5135

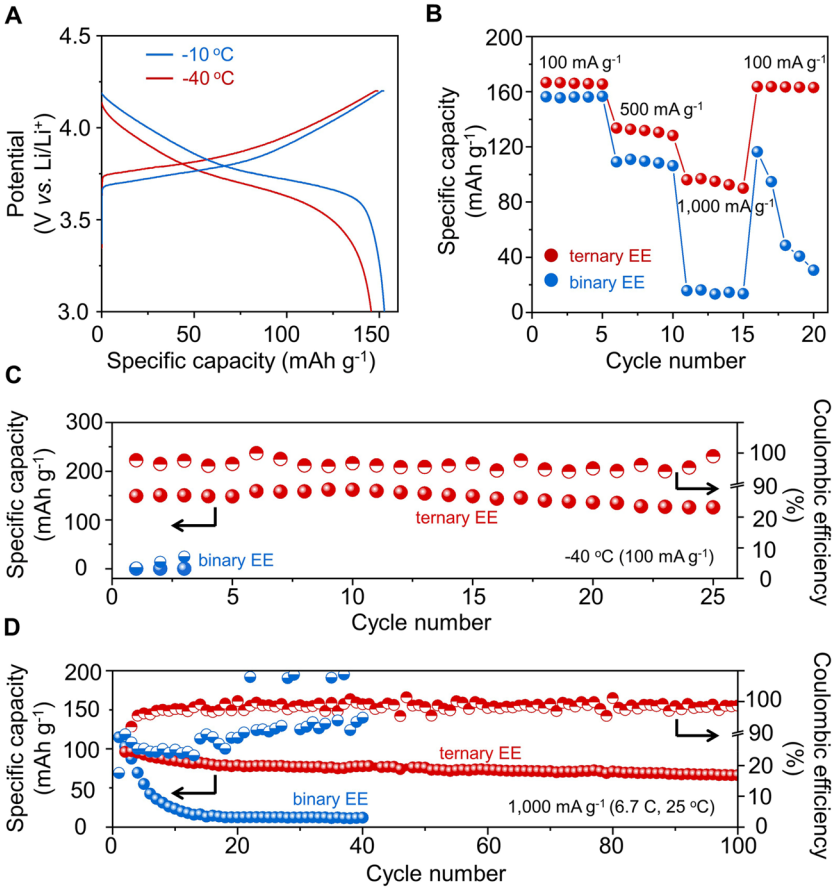

Figure 5. (A) Comparison of initial capacity enabled by ternary EE at −10 °C and −40 °C. (B) Comparison of discharge capacities between ternary EE and binary EE at varied current densities at 25 °C. (C) Cycling of the ternary EE at −40 °C in Li‖NCM622. (D) Cycling of ternary EE at 1,000 mA g^{-1} (6.7 C) in Li‖NCM622.

scanning calorimetry (DSC) was performed. Upon forming ternary EE, we observed the vanishing of melting from brush-PDMS (−40 °C), SN (−39 °C), and LiTFSI (236 °C, not shown), respectively, to the testing temperature below −80 °C (Figures 3A and S13). Therefore, the viscosity of ternary eutectics was reduced from 1.3 Pa·s in the binary EE to 1.0 Pa·s in the ternary EE at 25 °C (Figures 3B and S14). Such intermolecular interaction was supported by spectroscopic and simulation experiments carried out via molecular dynamics simulation, Raman spectroscopy, and ^{7}Li NMR and Fourier transform infrared (FT-IR) spectroscopy. Figure 3C shows a snapshot of the MD simulation of ternary EE at −40 °C in the inset. Comparative analysis of the radial distribution function (RDF, solid red line) and coordination number $n(r)$ showed that Li^+ possessed a coordination number of 3.1 with C≡N in SN in the ternary EE, whereas a higher coordination of 3.7 was observed in binary EE. These results suggest that the addition of brush-PDMS reduced the direct coordination between SN and LiTFSI in ternary EE, competitively binding with the central Li^+ based on Lewis acid−base interactions.

The Raman shift of the characteristic C≡N peak at 2248 cm^{-1} is sensitive to the coordination environment in the electrolyte. As shown in Figure 3D, SN in binary EE interacted with Li^+ and exhibited a blue shift to 2260 cm^{-1} compared with uncoordinated SN. The wavenumber of C≡N was further shifted in ternary EE owing to indirect brush-PDMS···Li^+ binding, which presumably reduced Li^+ coordination with SN and yielded a red shift to 2252 cm^{-1}. The ternary C≡N···Li^+···brush-PDMS coordination was substantiated in ^{7}Li NMR by a downfield shift of lithium signal in ternary EE (−0.701 ppm) relative to binary EE (−0.716 ppm). Additionally, the shoulder peak corresponding to the interface between SN and LiTFSI in binary electrolyte[36] was found to disappear upon the addition of brush-PDMS, corroborating the enhanced coordination enabled by brush-PDMS and the formation of a ternary eutectics, as is shown in Figure 3E. Furthermore, S═O vibration of $TFSI^-$ anions in FT-IR exhibited a higher degree of free $TFSI^-$ at 1330 cm^{-1} compared with coordinated $TFSI^-$ at 1350 cm^{-1}, where more Li^+−electrolyte binding would repel $TFSI^-$ anions from the primary Li^+ solvation sheath.[37] As deconvolved in Figure 3F, the ratio of free $TFSI^-$ in total $TFSI^-$ was reduced from 68.3% in binary EE to 53.1% in ternary EE, attributed to the change of solvation environment of Li^+ caused by steric hindrance of polymers. This result is in correspondence with our previous finding on reduced solvation caused by polymer-driven weak Li^+−electrolyte binding.[29] The competitive ternary coordination involving bulky brush-PDMS could lessen strong solvation of Li^+ with SN, which is potentially beneficial to facilitate Li^+ desolvation and form anion-derived SEI.[8,37,38]

Stabilized Interface at Li Anode. As a result, the Li−electrolyte interface was effectively stabilized in ternary EE at varied areal capacities and temperatures (Figures S21 and S22). The symmetric Li‖Li cells containing ternary EE afforded long-term cycling at a striking areal capacity of 30.0 mAh cm^{-2} with no sign of dendrites-induced charge

https://doi.org/10.1021/acsenergylett.3c01558
ACS Energy Lett. 2023, 8, 5128−5135

polarization for more than 3,000 h, where binary EE completely failed to operate (Figure 4A). Similar improvement was also found at reduced temperatures of −10 °C for ternary EE, which showed a constant and low average overpotential at 60 mV during continuous operation, while binary EE exhibited extremely high voltage hysteresis as a comparison (Figure 4B). Enhanced Coulombic efficiencies were observed in Li||Cu cells for ternary EE, in contrast to the inferior performance of binary EE as well as the conventional 1 M $LiPF_6$ in EC/DMC electrolyte (Figures S23 and S24). The low-temperature morphology was investigated by SEM characterizations. As shown in Figure 4C, dendrite nucleation was inhibited and uniform Li deposition along the electrode surface was observed in ternary EE, while binary EE yielded uneven and thickened deposition layer. The favorable morphological change was supported by X-ray photoelectron spectroscopy (XPS), where a dominating peak of LiF (685.5 eV) was present for ternary EE, indicative of a robust SEI. The generation of LiF-rich SEI was ascribed to the engagement of $TFSI^-$ in Li^+ solvation and contribution to SEI formation,[8,37] which agrees well with the $TFSI^-$ coordination result in FT-IR and was evidenced by the presence of C−F (687.3 eV), O═S═O (169.1 eV), and Li_2S (161.2 eV) peaks corresponding to $TFSI^-$ decomposition. Such anion-derived SEI avoided repetitive SEI repairing and generated a thin SEI observed by Li 1s XPS depth-profile analysis (4D-4E), where LiF-based SEI species (55.6 eV) gradually disappeared with appearance of Li^0 metal anode (54.7 eV) within 30 nm in ternary EE, suggesting a notable reduction of SEI thickness in comparison to that in binary EE (>80 nm).[13]

We further quantified the desolvation energy ($E_{a,de}$) at the interface, which is a critical step during charge transfer at the interface and can be decoupled from that of Li^+ migration through SEI ($E_{a,SEI}$) according to established studies by electrochemical impedance spectroscopy (EIS).[9,39] In contrast to the 99 kJ mol^{-1} obtained for binary EE, the interfacial resistance was significantly lowered in ternary EE, resulting in a reduced desolvation energy barrier ($E_{a,de}$ = 40.9 kJ mol^{-1}, Figure 4F). Moreover, the activation energy of Li^+ migration through SEI was also found to decrease in ternary EE ($E_{a,SEI}$ = 45.7 kJ mol^{-1}, Figure 4G), agreeing well with the formation of a favorable SEI at the electrode/electrolyte interface (Figure S25).

Low-Temperature and Fast-Charging Performance of LMBs. Owing to formation of ternary EE that could effectively accelerate kinetics in both mass transport and Li^+ charge transfer at the interface, Li||ternary EE||NCM622 cells were assembled. We performed battery testing at varied temperatures and C-rates with consistent charging and discharging conditions. The battery exhibited a high initial specific capacity of 174 mAh g^{-1} at 10 mA g^{-1} and 25 °C (Figure S27), while reducing the temperatures to −10 °C still yielded specific discharge capacities of 153 mAh g^{-1}, accounting for 88% of room-temperature capacity (Figure 5A). By increasing the current density to 100 mA g^{-1}, the ternary EE exhibited an initial discharge capacity of 150 mAh g^{-1} at −10 °C in Li|| NCM622 (Figure S28). When cooling further to −40 °C, ternary EE delivered an excellent initial capacity of 149 mAh g^{-1}, representing 85% of its room-temperature capacity, which remained to be 125 mAh g^{-1} after 25 cycles (Figure 5C). This performance is on par with or better than recent improvements achieved by small molecular electrolyte systems at low-T (Table S3). Subsequently, the comparison of rate capability between binary EE and ternary EE at different current densities (100−1,000 mA g^{-1}, Figure 5B) as well as the long-term high-rate charging and discharging cycling performance were evaluated, where concentration polarization could significantly increase and electrolyte kinetics determines deployable capacity. Ternary EE showed a high initial capacity of 167 mAh g^{-1} when charged at 100 mA g^{-1} and 25 °C (Figure S29), slightly better than that of binary EE (156 mAh g^{-1}). The long-term cycling showed stabilized cycling for ternary EE, which afforded capacity retention of 87% with a high CE of 99% over 100 cycles. When current rate was increased from 500 mA g^{-1} (3.3 C, 12 min recharging, Figure S30) to 1,000 mA g^{-1} at 25 °C (6.7 C, 6 min recharging, Figure 5D), we observed appreciable retention of initial capacity for ternary EE (96 mAh g^{-1}), where 79 mAh g^{-1} was maintained after 100 cycles with average CE of 98%. This performance is far beyond that for binary EE (13 mAh g^{-1}) which exhibits severe degradation owing to parasitic reactions of nitrile groups against Li anode and represents excellent performance compared with a variety of existing lithium battery systems at high rates.[6]

In summary, we developed a nonflammable polysiloxane-based ternary eutectic electrolyte that allowed LMB operations at low-temperature and high-rate conditions. The introduction of brush-PDMS to form a ternary EE surprisingly boosted the conductivity by almost three times at low temperatures, instead of slowing down ion conduction, as common polymers that would prohibit dynamically demanding battery operations. As a result, favorable mass transport and interfacial kinetics were observed with an effectively stabilized Li deposition. Stable long-term cycling in Li||NCM622 full cells at −40 °C and 1,000 mA g^{-1} was achieved with high discharge capacity retention. The novel findings of polysiloxanes mark promising progress at extreme conditions and might stimulate more exciting research by leveraging nonflammable and nonvolatile polymers to tune solvation structure and regulate ion transport kinetics from a molecular design perspective.

■ ASSOCIATED CONTENT

Supporting Information

The Supporting Information is available free of charge at https://pubs.acs.org/doi/10.1021/acsenergylett.3c01558.

Synthetic method, ^1H NMR spectra, optical images of eutectic electrolytes, CV curves, EIS data, rheological data, SEM images, Raman spectra, FT-IR spectra, XPS spectra, DFT calculation method (PDF)

■ AUTHOR INFORMATION

Corresponding Authors

Yuan Yang − *Department of Applied Physics and Applied Mathematics, Columbia University, New York, New York 10027, United States;* orcid.org/0000-0003-0264-2640; Email: yy2664@columbia.edu

Xinrong Lin − *School of Chemical Science and Technology, Yunnan University, Kunming 650091, China; Division of Natural and Applied Sciences, Duke Kunshan University, Kunshan, Jiangsu 215306, China;* orcid.org/0000-0003-1157-0175; Email: xl422@duke.edu

Authors

Weiping Li − *School of Chemical Science and Technology, Yunnan University, Kunming 650091, China; Division of Natural and Applied Sciences, Duke Kunshan University,*

https://doi.org/10.1021/acsenergylett.3c01558
ACS Energy Lett. 2023, 8, 5128−5135

Kunshan, Jiangsu 215306, China; orcid.org/0000-0002-0210-5119

Peng Wen − *School of Chemical Science and Technology, Yunnan University, Kunming 650091, China; State Key Laboratory of Molecular Engineering of Polymers, Department of Macromolecular Science, Fudan University, Shanghai 200433, China*

Yang Ren − *School of Chemical Science and Technology, Yunnan University, Kunming 650091, China*

Wen Xie − *School of Chemical Science and Technology, Yunnan University, Kunming 650091, China*

Jun Lin − *School of Chemical Science and Technology, Yunnan University, Kunming 650091, China;* orcid.org/0000-0002-2087-6013

Mao Chen − *State Key Laboratory of Molecular Engineering of Polymers, Department of Macromolecular Science, Fudan University, Shanghai 200433, China;* orcid.org/0000-0002-5504-3775

Complete contact information is available at: https://pubs.acs.org/10.1021/acsenergylett.3c01558

Notes

The authors declare no competing financial interest.

■ ACKNOWLEDGMENTS

This research was financially supported by the NSFC (nos. 22065037 and 52003231), Yunnan Fundamental Research Projects (202201AW070015). Yuan Yang acknowledges support from Columbia University.

■ REFERENCES

(1) Gupta, A.; Manthiram, A. Designing Advanced Lithium-Based Batteries for Low-Temperature Conditions. *Adv. Energy Mater.* **2020**, *10*, No. 2001972.

(2) Xu, K. Nonaqueous Liquid Electrolytes for Lithium-Based Rechargeable Batteries. *Chem. Rev.* **2004**, *104*, 4303−4418.

(3) Lin, X.; Salari, M.; Arava, L. M.; Ajayan, P. M.; Grinstaff, M. W. High temperature electrical energy storage: advances, challenges, and frontiers. *Chem. Soc. Rev.* **2016**, *45*, 5848−5887.

(4) Lin, D.; Liu, Y.; Cui, Y. Reviving the lithium metal anode for high-energy batteries. *Nat. Nanotechnol.* **2017**, *12*, 194−206.

(5) Zhang, N.; Deng, T.; Zhang, S.; Wang, C.; Chen, L.; Wang, C.; Fan, X. Critical Review on Low-Temperature Li-Ion/Metal Batteries. *Adv. Mater.* **2021**, No. e2107899.

(6) Liu, Y.; Zhu, Y.; Cui, Y. Challenges and opportunities towards fast-charging battery materials. *Nat. Energy* **2019**, *4*, 540−550.

(7) Zhang, S. S.; Xu, K.; Jow, T. R. The low temperature performance of Li-ion batteries. *J. Power Sources* **2003**, *115*, 137−140.

(8) Holoubek, J.; Liu, H.; Wu, Z.; Yin, Y.; Xing, X.; Cai, G.; Yu, S.; Zhou, H.; Pascal, T. A.; Chen, Z.; Liu, P. Tailoring electrolyte solvation for Li metal batteries cycled at ultra-low temperature. *Nat. Energy* **2021**, *6*, 303−313.

(9) Li, Q.; Lu, D.; Zheng, J.; Jiao, S.; Luo, L.; Wang, C. M.; Xu, K.; Zhang, J. G.; Xu, W. Li(+)-desolvation dictating Lithium-ion battery's low-temperature performances. *ACS Appl. Mater. Interfaces* **2017**, *9*, 42761−42768.

(10) Rustomji, C. S.; Yang, Y.; Kim, T. K.; Mac, J.; Kim, Y. J.; Caldwell, E.; Chung, H.; Meng, Y. S. Liquefied gas electrolytes for electrochemical energy storage devices. *Science* **2017**, *356*, No. eaal4263.

(11) Smart, M. C.; Ratnakumar, B. V.; Whitcanack, L. D.; Chin, K. B.; Surampudi, S.; Croft, H.; Tice, D.; Staniewicz, R. Improved low-temperature performance of lithium-ion cells with quaternary carbonate-based electrolytes. *J. Power Sources* **2003**, *119*−*121*, 349−358.

(12) Dong, X.; Guo, Z.; Guo, Z.; Wang, Y.; Xia, Y. Organic Batteries Operated at − 70°C. *Joule* **2018**, *2*, 902−913.

(13) Fan, X.; Ji, X.; Chen, L.; Chen, J.; Deng, T.; Han, F.; Yue, J.; Piao, N.; Wang, R.; Zhou, X.; Xiao, X.; Chen, L.; Wang, C. All-temperature batteries enabled by fluorinated electrolytes with non-polar solvents. *Nat. Energy* **2019**, *4*, 882−890.

(14) Dong, X.; Lin, Y.; Li, P.; Ma, Y.; Huang, J.; Bin, D.; Wang, Y.; Qi, Y.; Xia, Y. High-Energy Rechargeable Metallic Lithium Battery at −70 °C Enabled by a Cosolvent Electrolyte. *Angew. Chem., Int. Ed.* **2019**, *58*, 5623−5627.

(15) Cheng, Q.; Xu, W.; Qin, S.; Das, S.; Jin, T.; Li, A.; Li, A. C.; Qie, B.; Yao, P.; Zhai, H.; Shi, C.; Yong, X.; Yang, Y. Full Dissolution of the Whole Lithium Sulfide Family (Li2 S8 to Li2 S) in a Safe Eutectic Solvent for Rechargeable Lithium-Sulfur Batteries. *Angew. Chem., Int. Ed.* **2019**, *58*, 5557−5561.

(16) Jaumaux, P.; Liu, Q.; Zhou, D.; Xu, X.; Wang, T.; Wang, Y.; Kang, F.; Li, B.; Wang, G. Deep Eutectic Solvent-Based Self-Healing Polymer Electrolyte for Safe and Long-Life Lithium Metal Batteries. *Angew. Chem., Int. Ed.* **2020**, *59*, 9134−9142.

(17) Yang, W.; Du, X.; Zhao, J.; Chen, Z.; Li, J.; Xie, J.; Zhang, Y.; Cui, Z.; Kong, Q.; Zhao, Z.; Wang, C.; Zhang, Q.; Cui, G. Hydrated Eutectic Electrolytes with Ligand-Oriented Solvation Shells for Long-Cycling Zinc-Organic Batteries. *Joule* **2020**, *4*, 1557−1574.

(18) Lee, M. J.; Han, J.; Lee, K.; Lee, Y. J.; Kim, B. G.; Jung, K. N.; Kim, B. J.; Lee, S. W. Elastomeric electrolytes for high-energy solid-state lithium batteries. *Nature* **2022**, *601*, 217−222.

(19) Zhang, C.; Zhang, L.; Yu, G. Eutectic Electrolytes as a Promising Platform for Next-Generation Electrochemical Energy Storage. *Acc. Chem. Res.* **2020**, *53*, 1648−1659.

(20) Xu, B.; Zhai, H.; Liao, X.; Qie, B.; Mandal, J.; Gong, T.; Tan, L.; Yang, X.; Sun, K.; Cheng, Q.; Chen, M.; Miao, Y.; Wei, M.; Zhu, B.; Fu, Y.; Li, A.; Chen, X.; Min, W.; Nan, C.-W.; Lin, Y.-H.; Yang, Y. Porous insulating matrix for lithium metal anode with long cycling stability and high power. *Energy Storage Materials* **2019**, *17*, 31−37.

(21) Zhou, D.; Shanmukaraj, D.; Tkacheva, A.; Armand, M.; Wang, G. Polymer electrolytes for lithium-based batteries: advances and prospects. *Chem.* **2019**, *5*, 2326−2352.

(22) Chen, J.; Deng, X.; Gao, Y.; Zhao, Y.; Kong, X.; Rong, Q.; Xiong, J.; Yu, D.; Ding, S. Multiple Dynamic Bonds-Driven Integrated Cathode/Polymer Electrolyte for Stable All-Solid-State Lithium Metal Batteries. *Angew. Chem., Int. Ed.* **2023**, *62*, No. e202307255.

(23) Ma, M.; Shao, F.; Wen, P.; Chen, K.; Li, J.; Zhou, Y.; Liu, Y.; Jia, M.; Chen, M.; Lin, X. Designing Weakly Solvating Solid Main-Chain Fluoropolymer Electrolytes: Synergistically Enhancing Stability toward Li Anodes and High-Voltage Cathodes. *ACS Energy Lett.* **2021**, *6*, 4255−4264.

(24) Li, A.; Liao, X.; Zhang, H.; Shi, L.; Wang, P.; Cheng, Q.; Borovilas, J.; Li, Z.; Huang, W.; Fu, Z.; Dontigny, M.; Zaghib, K.; Myers, K.; Chuan, X.; Chen, X.; Yang, Y. Nacre-Inspired Composite Electrolytes for Load-Bearing Solid-State Lithium-Metal Batteries. *Adv. Mater.* **2019**, *32*, No. e1905517.

(25) Jaumaux, P.; Wu, J.; Shanmukaraj, D.; Wang, Y.; Zhou, D.; Sun, B.; Kang, F.; Li, B.; Armand, M.; Wang, G. Non-Flammable Liquid and Quasi-Solid Electrolytes toward Highly-Safe Alkali Metal-Based Batteries. *Adv. Funct. Mater.* **2021**, *31*, No. 2008644.

(26) Zhai, H.; Gong, T.; Xu, B.; Cheng, Q.; Paley, D.; Qie, B.; Jin, T.; Fu, Z.; Tan, L.; Lin, Y.-H.; Nan, C.-W.; Yang, Y. Stabilizing Polyether Electrolyte with a 4 V Metal Oxide Cathode by Nanoscale Interfacial Coating. *ACS Appl. Mater. Interfaces* **2019**, *11*, 28774−28780.

(27) Lopez, J.; Mackanic, D. G.; Cui, Y.; Bao, Z. Designing polymers for advanced battery chemistries. *Nat. Rev. Mater.* **2019**, *4*, 312−330.

(28) Cheng, Q.; Miao, Y.; Liu, Z.; Borovilas, J.; Zhang, H.; Liu, S.; Wang, H.; Chen, X.; Chen, L.-Q.; Min, W.; Yang, Y. Stabilizing Lithium Metal Anode by Ion Depletion-Induced Phase Transformation in Polymer Electrolytes. *Joule* **2022**, *6*, 2372−2389.

(29) Wen, P.; Liu, Y.; Mao, J.; Liu, X.; Li, W.; Ren, Y.; Zhou, Y.; Shao, F.; Chen, M.; Lin, J.; Lin, X. Tuning desolvation kinetics of in-

situ weakly solvating polyacetal electrolytes for dendrite-free lithium metal batteries. *J. Energy Chem.* **2023**, *79*, 340−347.
(30) Xu, J.; Ji, X.; Zhang, J.; Yang, C.; Wang, P.; Liu, S.; Ludwig, K.; Chen, F.; Kofinas, P.; Wang, C. Aqueous electrolyte design for super-stable 2.5 V LiMn2O4 || Li4Ti5O12 pouch cells. *Nature Energy* **2022**, *7*, 186−193.
(31) Liang, H. P.; Zarrabeitia, M.; Chen, Z.; Jovanovic, S.; Merz, S.; Granwehr, J.; Passerini, S.; Bresser, D. Polysiloxane-Based Single-Ion Conducting Polymer Blend Electrolyte Comprising Small-Molecule Organic Carbonates for High-Energy and High-Power Lithium-Metal Batteries. *Adv. Energy Mater.* **2022**, *12*, 2200013.
(32) Alarco, P.-J.; Abu-Lebdeh, Y.; Abouimrane, A.; Armand, M. The plastic-crystalline phase of succinonitrile as a universal matrix for solid-state ionic conductors. *Nat. Mater.* **2004**, *3*, 476−481.
(33) Sun, H.; Xie, X.; Huang, Q.; Wang, Z.; Li, Y.; Li, H.; Qiu, J.; Zhou, W. Fluorinated Poly-oxalate Electrolytes Stabilizingboth Anodeand Cathode Interfaces for All-Solid-State Li/NMC811 Batteries. *Angew. Chem., Int. Ed.* **2021**, *60*, 18335−18343.
(34) Wang, Q.; Zhang, H.; Cui, Z.; Zhou, Q.; Shangguan, X.; Tian, S.; Zhou, X.; Cui, G. Siloxane-based polymer electrolytes for solid-state lithium batteries. *Energy Storage Mater.* **2019**, *23*, 466−490.
(35) Xia, S.; Wu, X.; Zhang, Z.; Cui, Y.; Liu, W. Practical Challenges and Future Perspectives of All-Solid-State Lithium-Metal Batteries. *Chem.* **2019**, *5*, 753−785.
(36) Zheng, J.; Tang, M.; Hu, Y. Y. Lithium Ion Pathway within Li7 La3 Zr2 O12 -Polyethylene Oxide Composite Electrolytes. *Angew. Chem., Int. Ed.* **2016**, *55*, 12538−12542.
(37) Yu, Z.; Wang, H.; Kong, X.; Huang, W.; Tsao, Y.; Mackanic, D. G.; Wang, K.; Wang, X.; Huang, W.; Choudhury, S.; Zheng, Y.; Amanchukwu, C. V.; Hung, S. T.; Ma, Y.; Lomeli, E. G.; Qin, J.; Cui, Y.; Bao, Z. Molecular design for electrolyte solvents enabling energy-dense and long-cycling lithium metal batteries. *Nat. Energy* **2020**, *5*, 526−533.
(38) Jia, M.; Wen, P.; Wang, Z.; Zhao, Y.; Liu, Y.; Lin, J.; Chen, M.; Lin, X. Fluorinated bifunctional solid polymer electrolyte synthesized under visible light for stable lithium deposition and dendrite-free all-solid-state batteries. *Adv. Funct. Mater.* **2021**, *31*, No. 2101736.
(39) Yan, C.; Li, H.-R.; Chen, X.; Zhang, X.-Q.; Cheng, X.-B.; Xu, R.; Huang, J.-Q.; Zhang, Q. Regulating the Inner Helmholtz Plane for Stable Solid Electrolyte Interphase on Lithium Metal Anodes. *J. Am. Chem. Soc.* **2019**, *141*, 9422−9429.

https://doi.org/10.1021/acsenergylett.3c01558
ACS Energy Lett. 2023, 8, 5128−5135